JCTC Journal of Chemical Theory and Computation

# Theoretical Study on the Redox Cycle of Bovine Glutathione Peroxidase GPx1: p$K_a$ Calculations, Docking, and Molecular Dynamics Simulations

Syed Tahir Ali, Sajid Jahangir, Sajjad Karamat, Walter M. F. Fabian, Krzysztof Nawara, and Juraj Kóňa*

*Institute of Chemistry, Karl Franzens University, Graz, Heinrichstrasse 28, A-8010 Graz, Austria, Department of Chemistry, Federal Urdu University of Arts, Science and Technology, Gulshan-e-Iqbal Science Campus, Karachi, Sindh, Pakistan, and Institute of Chemistry, Center for Glycomics, Slovak Academy of Sciences, Dúbravska cesta 9, 845 38 Bratislava, Slovak Republic*

Received July 2, 2009

**Abstract:** Three approaches of computational chemistry [quantum mechanics (QM) calculations, docking, and molecular dynamics (MD) simulations] were used to investigate the redox cycle of bovine erythrocyte glutathione peroxidase from class 1 (GPx1, EC 1.11.1.9). The p$K_a$ calculations for two redox states of the active-site selenocysteine of GPx1 (selenol, Sec45−SeH, and selenenic acid, Sec45−SeOH) were estimated using a bulk solvent model (B3LYP-IEFPCM and B3LYP-CPCM-COSMO-RS). The calculated p$K_a$ values of Sec45−SeH and Sec45−SeOH were corrected via a simple linear fit to a training set of organoselenium compounds, which consisted of aliphatic selenols and aromatic selenenic acids with available experimental p$K_a$ values. Based on docking calculations, binding sites for both molecules of the cofactor glutathione (GSH) are described. MD simulations on the dimer of GPx1 have been performed for all chemical states of the redox cycle: without GSH and with one or two molecules of GSH bound at the active site. Conformational analyses of MD trajectories indicate high mobility of the Arg177 and His79 residues. These residues can approach the vicinity of Sec45 and take part in the catalytic mechanism. On the basis of the calculated data, new atomistic details for a generally accepted mechanism of GPx1 are proposed.

## 1. Introduction

Glutathione peroxidase (GPx, EC 1.11.1.9) was the first selenoprotein identified in mammals.[1] It protects cells from oxidative damage by catalyzing the reduction of $H_2O_2$, lipidhydroperoxides, and other organic peroxides, using glutathione ($\gamma$-glutamylcysteinylglycin, GSH) as the reducing substrate.[2] The X-ray structure of the tetrameric *Bos taurus* erythrocyte glutathione peroxidase from class 1 (GPx1) showed two asymmetric units containing two dimers, each with one selenocysteine residue (Sec) per active site at the monomer unit.[3] The active sites of GPx1 are found in flat depressions on the molecular surface and are located at a contact region of the dimer units. Biochemical,[2−7] kinetic[8] and crystallographic[3,7] studies have suggested that the Sec residue directly participates in the catalytic process of the reduction of hydroperoxide by GPx. It has been experimentally suggested that the catalytically active form of the enzyme is the selenolate anion (E−Se$^-$).[3,4] The proposed mechanism of the overall catalytic cycle is shown in Figure 1a. In the first redox step, E−Se$^-$ is oxidized to the selenenic acid (E−SeOH) with the accompanying reduction of a hydroperoxide substrate to a corresponding alcohol. In the second step, the E−SeOH reacts with GSH to produce a selanyl sulfide adduct (E−SeSG). In the third step, a second molecule of GSH attacks E−SeSG to regenerate the active form of the enzyme, and the oxidized form of GSH (GSSG) is formed as a byproduct. This step has been suggested to

* Corresponding author. Telephone: +421-2-59410322. Fax: +421-2-59410222. E-mail: chemkona@savba.sk.

10.1021/ct9003355 
Published on Web 04/22/2010

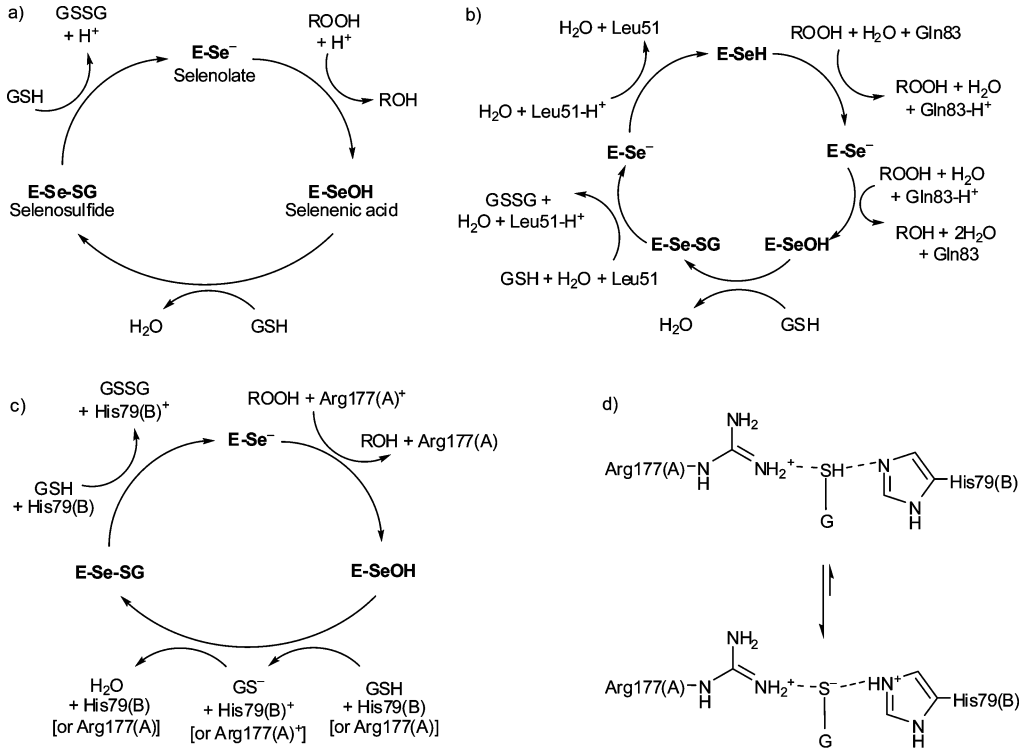


***Figure 1.*** (a) Catalytic cycle of GPx1 after Epp et al.[3] The resting state of Sec is selenolate. A proton donor and acceptor in the first and third redox steps are not known. (b) Catalytic cycle of GPx3 proposed by Prabhakar et al.[10] and tested by density functional theory (DFT) calculations. The resting state of Sec is selenol. The concomitant proton transfers occur between Sec and amide nitrogen (side chain) of Gln83 and between GSH and amide nitrogen (backbone) of Leu51, facilitated by solvent water molecules. (c) A proposed catalytic mechanism of GPx1 in this work. The His79(B) and Arg177(A) residues play a role of catalytic acid/base based on docking, MD simulations, and p$K_a$ calculations at the QM level. (d) In the presence of Arg177(A), a p$K_a$ value of the thiol group of GSH can be depressed below 7, and the equilibrium shifted on the side of the thiolate state of GSH in the presence of His79(B).

be the rate-determining step of the entire mechanism.[9] As can be seen in the reaction scheme (Figure 1), a proton must be supplied for the first redox step and be abstracted in the third reaction step to maintain overall stoichiometry of the catalytic process. The mode of action of these proton transfers is not clear because no ionizable amino acid residues were found in the proximity of the Sec reaction center. Recently, a redox mechanism based on the proton transfer via solvent water molecules was proposed for human plasma glutathione peroxidase 3 (GPx3)[10−12] and for the redox reactions of organoselenium compounds[13−16] using quantum mechanics (QM) calculations. In the proposed mechanism for GPx3[10−12] (Figure 1b), water molecules participate in proton exchange between the selenol (and thiol groups) of selenocysteine (and glutathione) and the protein backbone. This is based on the assumption that the resting form of Sec is selenol, rather than the experimentally proposed selenolate state,[3,4] e.g., p$K_a$ value of Sec at GPx3 should be higher than 7 according to this mechanism. The mechanism had reasonable kinetics parameters, similar to those found for the redox reactions of selenocysteine,[17] organic selenols,[13,14,18−20] and thiols.[21−23]

The selenolate state of the Sec residue, rather than selenol, is further supported by its lower p$K_a$ value of 5.3[24] compared with cysteine (8.3).[2,25] Moreover, the selenolate state of the active-site Sec in selenosubtilisin was validated by NMR experiments (p$K_a$ < 4).[26] In contrast to the active site of the selenosubtilisin,[27] which consists of the Sec−His−Asp triad, no ionizing residues in direct interaction with the active-site Sec were found in the available crystal structures of GPx.[3,7,28,29] The ionizing Arg and His residues do place in the active site with a radius of 6−10 Å from Sec45 in GPx1. The His79 is located in the contact dimer region.[3] The sequence His79−Lys84, from the monomer unit B, participates at the active site of the monomer unit A and vice versa, the sequence from monomer A is involved at the active site of the monomer B. When GPx1 was treated with ammonium peroxodisulphate, loss of enzymatic activity with presumably His79 complexed with peroxodisulphate, was found as a major observation.[3] Difference Fourier analysis of the corresponding derivative revealed a positive difference density maximum, stretching symmetrically across the local axis at the positions of residues interpreted as His79(A) and His79(B). Presumably these histidine residues can influence the catalytic process, but this phenomenon is not understood in molecular terms at present.[3] Several other studies have demonstrated a catalytic role of the histidine in cysteine and selenocysteine redox proteins,[27,30−33] as thioredoxin reductases[35−37] or an OxyR transcription factor.[38,39]

Because the crystal structures of glutathione peroxidases present a nonreactive oxidized seleninic acid state (E−SeOO$^-$) or a Gly (or Ala) mutant of the Sec residue, we speculate that the position of side chains of the active-site Arg and His residues could be different in vivo compared with the crystal structures, mainly in the presence of one or

***Table 1.*** Enzyme and Cofactor Configurations Used in the Docking and MD Simulations[a]

| | Sec45(A), Sec45(B) | His79(A), His79(B) | GSH (in A) | Sec45(A), Sec45(B) | His79(A), His79(B) | Asn75−Gln81(A), Asn75−Gln81(B) |
|---|---|---|---|---|---|---|
| Dock01_GSH | R−SeH | His−N$\varepsilon$H$^0$ | R−SH | | | |
| Dock02_GSH_GSH | R−SeH | His−N$\varepsilon$H$^0$ | 2 R−SH | | | |
| Dock03_GSH_GS | R−SeH | His−N$\varepsilon$H$^0$ | RSH + R−S$^-$ | | | |
| Dock04_GSSH | R−SeH | His−N$\varepsilon$H$^0$ | R−S−S−R | | | |
| MD1_Se | R−Se$^-$ | His−N$\varepsilon$H$^0$ | No | − | + | + |
| | | | | − | − | − |
| MD1_S | R−S$^-$ | His−N$\varepsilon$H$^0$ | No | + | − | − |
| | | | | − | − | − |
| MD2_Se_GSH_GSH | R−Se$^-$ | His−N$\varepsilon$H$^0$ | 2 R−SH | − | − | − |
| | | | | − | + | + |
| MD3_SeOH | R−SeOH | His−N$\varepsilon$H$^0$ | No | − | + | − |
| | | | | − | − | − |
| MD4_SeO | R−SeO$^-$ | His−N$\varepsilon$H$^0$ | No | − | + | − |
| | | | | − | − | − |
| MD5_SeOH_GSH | R−SeOH | His−N$\varepsilon$H$^0$ | R−SH | + | + | + |
| | | | | − | + | + |
| MD6_SeO_GSH | R−SeO$^-$ | His−N$\varepsilon$H$^0$ | R−SH | − | + | + |
| | | | | + | + | + |
| MD7_SeO_GSH_GSH | R−SeO$^-$ | His−N$\varepsilon$H$^0$ | 2 R−SH | − | − | − |
| | | | | − | + | + |
| MD8_SeO_GSH_GS_HIP | R−SeO$^-$ | His−N$\varepsilon$H$^0$ | R−SH + R−S$^-$ | − | − | − |
| | | His$^+$(B) | | − | − | − |
| MD9_SeOH_GSH_GS_HIP | R−SeOH | His−N$\varepsilon$H$^0$ | R−SH + R−S$^-$ | − | − | + |
| | | His$^+$(B) | | − | + | + |
| MD10_SeSG | R−Se−S−R | His−N$\varepsilon$H$^0$ | No | − | − | + |
| | R−Se$^-$(B) | | | + | − | − |
| MD11_SeSG_GSH | R−Se−S−R | His−N$\varepsilon$H$^0$ | R−SH | − | − | − |
| | R−Se$^-$(B) | | | + | + | + |
| MD12_Se_GSSG | R−Se$^-$ | His−N$\varepsilon$H$^0$ | R−S−S−R | − | + | + |
| | | | | − | − | + |

[a] Plus brief results from the MD analyses concerning conformations of Sec45 and His79 and of the Asn75−Gln81 loop; (+) means structural changes compared with the X-ray structure of GPx1 (PDB ID: 1GP1), i.e., a flip of Sec45 or conformational change of the side chain of His79 or the Asn75−Gln81 loop.

two molecules of GSH bound at the active site (for example, two different conformations of the side chain of Arg180 in human GPx1 were observed, PDB ID: 2F8A).[40]

Here we calculated: (i) p$K_a$ values of Sec45 in two redox states to predict their forms at the physiological pH; and (ii) binding positions of both molecules of GSH, which revealed the importance of the Trp158, Arg177, and His79 for proper binding and reactivity of GSH. We also performed MD simulations on a nanosecond time scale to analyze the mobility of side chains of ionizable residues in the active site of GPx1. We will show that Arg177 and His79 can fill positions in the vicinity of selenol and thiol groups of Sec and GSH, respectively.

## 2. Computational Details

**2.1. Structural Models and Docking.** Based on the crystal structure of bovine GPx1 (PDB ID: 1GP1),[3] the 13 following configurations were simulated (Table 1) GPx1: with Sec in selenolate state without (MD1_Se) and with oxidized glutathione (MD12_Se_GSSG), with two molecules of GSH (MD2_Se_GSH_GSH), with Sec mutated to cysteine (MD1_S), in selenenic state (MD3_SeOH) and its ionized state (MD4_SeO), with one molecule of the reduced GSH (MD5_SeOH_GSH and MD6_SeO_GSH), with two molecules of GSH (combination of different ionization states of Sec45−SeOH, GSH and His79; MD7_SeO_GSH_GSH, MD8_SeO_GSH_GS_HIP, MD9_SeOH_GSH_GS_HIP), and in selanyl sulfide state without (MD10_SeSG) and with the reduced GSH (MD11_SeSG_GSH). Missing structural information on glutathione bound at the active site as well as on selanyl sulfide intermediate (E−SeSG) of GPx1 was added by means of docking calculations, employing the GLIDE program of the Schrödinger package.[41] One molecule of GSH was docked into the active site (Dock01_GSH, the selected configurations of the enzyme are compiled in Table 1), and then the second molecule of GSH (neutral GSH as well as ionized GS$^-$) was docked into the active site with the first molecule of glutathione already bound (Dock02_GSH_GSH and Dock03_GSH_GS). The oxidized form of glutathione was also docked into the active site (Dock04_GSSG). The selanyl sulfide intermediate of GPx1 for the MD10_SeSG and MD11_SeSG_GSH simulations was built from a docked pose (no. 16, Dock03_GSH_GS, see Figure 3e and a three-dimensional (3-D) structure in the Supporting Information) of the complex consisting of GPx1 and two molecules of the reduced form of GSH bound at the active site. In this complex a molecule of GSH (with a proximal position of its thiol group to the selenol group of Sec45 of GPx1) was covalently bound to Sec45 and subsequently minimized with the rest of the enzyme frozen at the crystallographic geometry using the MacroModel of the Schrödinger package.[42] For the constrained minimization, the OPLS2001 force field[43,44] was used for both enzyme and glutathione.

The GLIDE program[41,45] uses a hierarchical series of filters to search for possible locations of the ligand in the

active-site region of the receptor. The shape and properties of the receptor are represented on a grid by several sets of fields that provide progressively more accurate scoring of the ligand poses. Conformational flexibility is handled in GLIDE by an extensive conformational search, augmented by a heuristic screen. The scoring is carried out using the Schrödinger's discrete version of the ChemScore empirical scoring function. Much as for ChemScore itself, this algorithm recognizes favorable hydrophobic, hydrogen bonding, metal−ligand interactions, desolvation, and entropic effects and penalizes steric clashes.[46] For the docking calculations, default values of parameters were used. The receptor box for the docking conformational search was centered at Sec45 with a size of 30 × 30 × 30 Å, using partial atomic charges for the GPx1 receptor from the OPLS2001 force field.[43,44] The grid maps were created with no van der Waals radius and charge scaling for the atoms of the receptor. Flexible docking in standard,[45] which penalizes nonplanar conformation of amide bonds, was used for the glutathione ligands. The partial charges of the ligands were calculated at the ab initio level (for more details see the Section 2.2, MD simulations). The potential for nonpolar parts of the ligands was softened by scaling the van der Waals radii by a factor of 0.8 for atoms of the ligands with partial atomic charges less than specified cutoff of 0.15. The 5000 poses were kept per ligand for the initial docking stage with a scoring window of 100 kcal mol$^{-1}$ for keeping initial poses; and the best 400 poses were kept per ligand for energy minimization. The ligand poses with root-mean-square (rms) deviations less than 0.5 Å and maximum atomic displacement less than 1.3 Å were discarded as duplicates. One hundred ligand poses with the best docking score were saved for subsequent analyses using the MAESTRO viewer of the Schrödinger package.[47]

**2.2. MD Simulations.** Simulations with the explicit solvent model (TIP3P)[48] were performed with the standard AMBER 99 force field by means of the GROMACS 3.3.1[49] program package. For nonstandard amino acids and their ionized states (Sec−SeH, Sec−Se$^-$, Sec−SeOH, Sec−SeO$^-$, and Sec−SeSG) as well as for all states of the glutathione (GSH, GS$^-$, and GSSG), parameters were derived from either AMBER and GAFF force fields or built from data obtained by ab initio Hartree−Fock calculations[50] [HF/6-31G(d)] using the Gaussian 03 package.[51] The electrostatic potential fitting algorithm of Merz−Singh−Kollman scheme[52,53] was used [the keywords POP = MK IOP(6/33 = 2, 6/42 = 6)] to estimate atomic charges from the HF/6-31G(d) calculations (atom types, charges and added force field parameters are provided in the Supporting Information). The ionization states of the ionizing residues of the enzyme were predicted by the PropKa program,[54,55] considering an in vivo pH of 7 (calculated p$K_a$ values, and an output structure of GPx1 with predicted ionization configurations of the amino acid residues are available in the Supporting Information). Terminal and side-chain ionizing groups (amino and carboxyl) of glutathione molecules were treated in their ionized configurations (as $-NH_3^+$ or $-COO^-$) in all docking calculations and MD simulations.

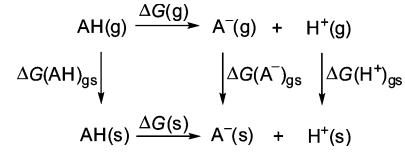


***Figure 2.*** Thermodynamic cycles of ionizing groups in aqueous solution.

The Berendsen algorithm[56] for temperature and the Parrinello−Rahman algorithm for pressure coupling, with coupling constants of $\tau_t = 1.0$ ps and $\tau_p = 1.0$ ps, were used at a constant temperature (300 K) and pressure (101.325 kPa). Periodic boundary conditions were used together with the particle-mesh Ewald (PME) method[57] for treating long-range electrostatics. A time step of 1.0 fs, with the LINCS algorithm[58] to constrain bonds involving hydrogens, was used along simulations with a 10 Å nonbonded cutoff, and the nonbonded pairlist was updated every 20 time steps. The simulations, preceded by initial minimizations (1000 steps), were carried out over 10 ns, and coordinates were saved for analysis every 1 ps. The protein was solvated by more than 14 000 TIP3P[48] water molecules in a box (66 × 108 × 71 Å) using the LEAP[59] program of the AMBER 8 package[60] (total number of atoms in the simulated system is ca. 50 000).

**2.3. p$K_a$ Calculations.** Based on the thermodynamic cycle[61−64] (Figure 2) p$K_a$ values were calculated using the following formulas:

$$pK_a = \Delta G/RT \ln 10$$

$$pK_a(s) = [\Delta G(g) + \Delta G(A^-)_{gs} - \Delta G(AH)_{gs} + \Delta G(H^+)_{gs}]/2.303RT$$

Here p$K_a$(s) is for a functional group in an aqueous solution. $G(H^+) = -6.28$ kcal mol$^{-1}$ and $\Delta G(H^+)_{gs} = -264.0$ kcal mol$^{-1}$ were derived experimentally,[65] where the standard state is 1 M [$\Delta G(H^+)_{gs}$ was calculated from the Tissandier et al.[63,66] value of $-265.9$ kcal mol$^{-1}$ and from the free energy change (1.89 kcal mol$^{-1}$ at 298 K) associated with moving from a standard state that uses the concentrations of 101.325 kPa in the gas phase and 1 M in the aqueous phase, to a standard state that uses a concentration of 1 M in both the gas and aqueous phases.]

A thermodynamic cycle in Figure 2 was used for the calculations of p$K_a$ values for a series of selenols (R−SeH, $n = 6$) and aryl selenenic acids (ArSeOH, $n = 5$) in aqueous solution.[61,63,70−73] Gibbs free energies were obtained by density functional theory (DFT) computations [B3LYP/6-31G(d,p)][74−76] using the Gaussian 03 package.[51] The solvent effect (aqueous solution) was estimated by the isoelectric focusing-polarizable continuum model (IEF-PCM).[69] Because of the lack of selenium parameters for the calculation of cavitation/dispersion/repulsion contributions, only the electrostatic component of the solvation energy was taken into account. The accuracy of the DFT methodology used was compared with DFT calculations with a larger basis set [6-31+G(d,p)[77,78] or aug-cc-pVDZ],[79] with an ab initio method [the second-order Møller−Plesset theory (MP2)][80] as well as with the another solvation model, CPCM variant

using COSMO-RS radii (CPCM-COSMO-RS)[81] (keyword SCRF = COSMORS with the default setting of the Gaussian 03 package[51]). Experimental p$K_a$ values are taken from the literature (selenols[2,82−84] and selenenic acids[85]).

The p$K_a$ values of Sec45 in selenol and selenenic acid forms in GPx1 were calculated based on a simple structural model, in which Sec45, in a conformation identical to that adopted in the enzyme, was reduced to isolated selenocysteine (or its selenenic acid form), and the effects of the aqueous solution were simulated by the above-mentioned PCM models. For these purposes, the structure of GPx1 was optimized using an enzyme model (built from a snapshot selected from the MD trajectory of MD1_Se). The four enzyme redox states, E−SeH, E−$Se^-$, E−SeOH, and E−$SeO^-$, were optimized at the hybrid quantum mechanics/molecular mechanics (QM/MM) level [the ONIOM with mechanic embedding (ME) scheme,[67,68] B3LYP/6-31G(d,p):Amber][11,12] using the Gaussian 03 package[51] (Gaussian ONIOM outputs of the optimized geometries are available in the Supporting Information). We used the ME scheme since optimization of GPx3 with the ONIOM scheme with the electrostatic embedding (EE) did not improve the results and gave a slightly larger rms deviation when the ONIOM geometries were compared with the X-ray structure of the enzyme.[12] ONIOM-ME does not include the exact electrostatic interaction between the electron density and the point charges in the protein environment, however, it includes electrostatic effects due to geometrical changes of amino acid residues and molecules of aqueous solvent involved in the QM part of the system (in our case: Sec45, Gly46, Thr47, Gln80, Trp158, Arg177, and 4 molecules of $H_2O$). The entire enzyme structure contains 246 molecules of water located in the active site (taken from the MD simulations), from which 4 molecules (located around the Sec45 residue) were treated at the QM level and the rest at the MM level.

The optimized geometries of the above-mentioned four redox states of Sec45 in the enzyme model were taken for the subsequent p$K_a$ calculations in the aqueous solution using the IEF-PCM[69] and CPCM-COSMO-RS[81] methods. The calculated p$K_a$ values were corrected via a simple linear fit to a training set of the organoselenium compounds according to the formula: p$K_a$ = k*[p$K_a$(raw)] + d (Table 4).

We also tried to evaluate effects of the protein environment on the calculated p$K_a$ values of Sec45 at the ONIOM-ME and ONIOM-EE as well as at the ONIOM-EE//ONIOM-ME levels. [However, unfitted p$K_a$ values of Sec45 based on the ONIOM schemes did not converge and had in some cases unreasonably high positive (>14, the calculations with basis set without diffuse functions) or low negative values (>−3, the calculations with the basis set augmented by the diffuse functions). Therefore, they will not be discussed in this work.]

## 3. Results and Discussion

**3.1. Docking.** The docking calculations were performed to provide missing structural information on both binding sites of GSH at the active site of GPx1. Because it is not clear at which redox state of GPx1 the two molecules of GSH bind into the active site, we used for our docking study GPx1 in its reduced selenol state. In the first experiment, we docked one molecule of the reduced GSH into a crystal geometry of the active site of GPx1 (Dock01_GSH). In the most favorable docking pose [with the best docking score of −5.4 kcal $mol^{-1}$, Figure 3b and Table S1 in the Supporting Information], GSH was positioned in a groove region, 7.5−11.0 Å apart from Sec45(A), where the thiol group of GSH was fitted in a hydrophobic area at the end of the groove [7.5 Å from the selenol group of Sec45(A)]. The hydrophobic pocket consists of Phe145(A), Trp158(A), and partially Arg177(A) [numbering according to the crystal structure of GPx1 (PDB ID: 1GP1)]. In the binding pose, a N-terminal amino group of the $\gamma$-glutamyl moiety of GSH interacts by hydrogen bonding with a side-chain carboxylate of Asp126 and the backbone carbonyl group of Ala129 (2.1 and 1.9 Å, see a 3-D structure in the Supporting Information), while a C-terminal carboxylate group of the glycin moiety of GSH interacts with Arg177 (1.9 Å). The tryptophan residue has been discussed by other authors[3,7,10,37,86] as an essential amino acid of the catalytic triad Sec−Gln−Trp in GPx, which modulates the selenium reaction center toward the feasible redox reactions. Based on our docking results, we believe that a catalytic Trp158 is mainly responsible for the proper binding of GSH. It provides the proper orientation of the thiol group of GSH close to the Sec45 reaction center. Therefore, it is evident from the docking pose that hydrophobic interactions between the tryptophan aromatic ring and the sulfur of GSH play a significant role in the redox mechanism of GPx1.

In the next experiment we docked another molecule of the reduced GSH into the active site of GPx1, with the first molecule of GSH already bound to the enzyme according to the previous docking calculations. GSH was docked into the enzyme either with a neutral (Dock02_GSH_GSH) or an ionized form (Dock03_GSH_GS) of its thiol group. For both ionization configurations similar docking poses for GSH were found. The second GSH was fitted in an enzyme region in the proximity of Sec45 (Figure 3a). The thiol group of GSH was placed into a small hydrophobic pocket located at the dimer contact surface near His79(B) (3.6 Å). (It should be noted that His79 from monomer A is not involved in the active site of this monomer, and instead is part of the active site of monomer B. And vice versa, His79 from monomer B is in the active site of monomer A.) Our results are in agreement with crystallographic experiments and their interpretation of the binding sites of GSH. When the reduced GPx1 was treated with an excess of GSH at pH 7, two binding sites of GSH per monomer of GPx1 were observed.[3] These binding sites were described by a positive, ill-defined, and noncontinuous difference electron density map (between Gpx1 and the complex GPx1:2GSH), with a maximum near to Sec45 and with a further density maximum stretching symmetrically from the dimer contact surface at the local axis [residues interpreted as His79(A) and His79(B)] into the inner part of each monomer.

An interatomic distance between thiol groups of the bound GSHs is 6.3 Å, while the distance between the thiol group of the GSH (interacted with Sec45) and the selenium atom

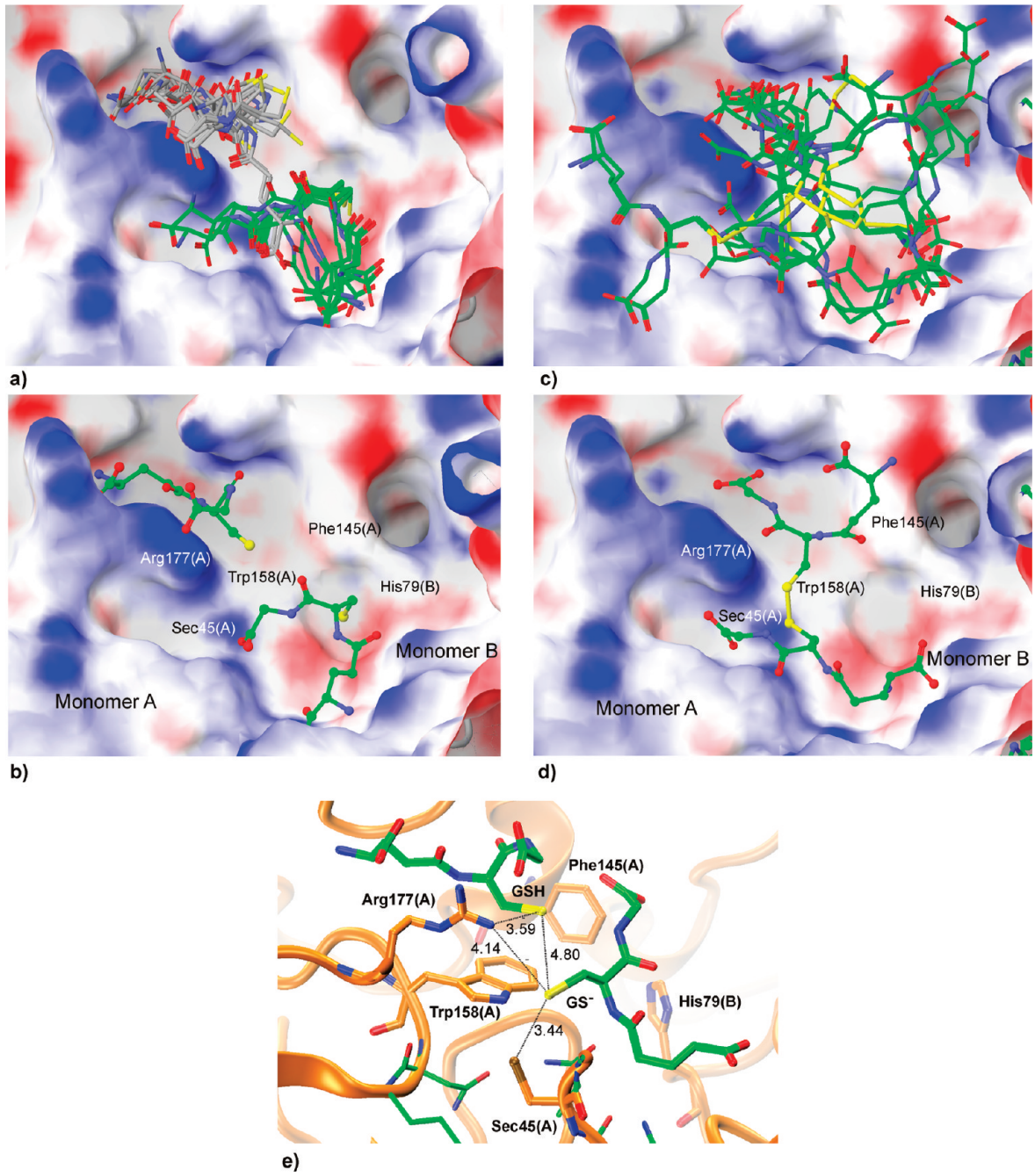


***Figure 3.*** (a) An active site of GPx1 (visualized by surfaces) with two docked molecules of GSH (the best 10 poses visualized for every molecule of GSH). The GSH molecule (gray) placed close to Arg177(A) is from the Dock01_GSH, and GSH (green) positioned next to His79(B) is from the Dock02_GSH_GSH calculations. (b) Poses of both GSHs with the best docking score. (c) The best 10 poses of the docked GSSG. (d) A pose of GSSG with the best docking score. (e) The binding pose no. 16 of $GS^-$ (Dock03_GSH_GS) with selected interatomic distances between sulfur (yellow), selenium (brown), and nitrogen (blue) atoms of GSH, $GS^-$, Sec45, and Arg177 (3-D structure in the Supporting Information). This pose could represent a starting reactive conformation for the second redox step of the GPx1 cycle.

of Sec45 is 8.0 Å. As can be seen from Figure 3b, after binding two molecules of GSH the active-site Sec45 residue is still not blocked (the analysis of the poses of GSHs with the best docking score) and could be oxidized to selenenic acid. Consequently, binding GSH prior to the formation of selenenic acid could protect Sec against the formation of higher oxidation states in an unwanted reaction with other molecules of the hydroperoxide substrate, i.e., the bound GSH can preferentially react with the selenenic acid intermediate and, thus, effectively compete with a hydroperoxide substrate. This assumption is indirectly supported by experiments with a radioactive GSH.[3] These demonstrated that GSH had been bound noncovalently to the reduced GPx1 and that its binding prior to the formation of any putative selanyl sulfide intermediate occurs via a reversible equilibrium as long as the system, consisting of the enzyme and GSH, was in the reduced state.[3]

Among the most preferable binding poses in the calculations with the ionized thiol group of GSH (pose no.16 with a docking score of $-3.1$ kcal $mol^{-1}$ and no. 20 ($-3.0$ kcal

mol$^{-1}$); for comparison the pose no. 1 possesses the best docking score of −4.2 kcal mol$^{-1}$], the binding poses of GSH with the thiolate oriented toward Sec45(A) (3.5 Å) still in vicinity of the thiol group of the first bound GSH (4.8 Å) and Arg177(A) (3.5 Å) [or His79(B) (4.8 Å)], were found (Figure 3e, see also 3-D structure in the Supporting Information). These poses could represent starting reactive conformations for the second and third redox step of the GPx1 cycle. The direct interaction between the side chain of His79(B) [or Arg177(A)] and the thiol group of GSH allowed us to consider them as catalytic residues involved in the redox mechanism of GPx1. They could assist in deprotonation of the thiol group of both GSHs to a more reactive thiolate (their role is also supported by our MD simulations and will be further discussed in the next section).

The docking study with oxidized glutathione (Dock04_GSSH) indicated a binding pose with the disulfide linkage of GSSG positioned close to Sec45 (4.5 Å) and placed in the vicinity of the Phe145-Trp158-Arg177 hydrophobic area (Figure 3d). GSSG was placed in the same regions as it was for the reduced GSHs in previous docking calculations but with a different position of its backbone (see 3-D structure in Supporting Information). For the oxidized GSSG, we observed a lower docking score compared with the reduced GSH (−6.5 kcal mol$^{-1}$ for GSSG versus −10.1 kcal mol$^{-1}$ for 2GSH). This is in agreement with the assumption that, after the last redox step, GSSG should be released from the active site to allow for binding with other molecules of hydroperoxide substrate and reduced GSH.

**3.2. MD Simulations.** The main goal of the simulations was to investigate the mobility of side chains of the active-site ionizing residues, mainly His79 and Arg177. These residues could facilitate deprotonation of the selenol as well as the thiol groups of Sec45 and GSH and increase the efficiency of the redox catalysis of GPx1. The MD simulations were performed on the enzyme dimer, and thus, we could simultaneously analyze conformational changes at the two active-sites of GPx1 and investigate a possible cooperation across the dimer interface. (It should be noted that both active sites in the dimer unit are located close to each other and separated by the contact region between the monomer units.)

In the crystal structure of GPx1, the active-site Sec45 residue (in the oxidized seleninic state, RSeOO$^-$) is located at the N-terminal end of an α-helix, which forms a $\beta\alpha\beta$ substructure together with the two adjacent parallel $\beta$ strands. In most MD trajectories (in 21 of overall 26 active sites, Table 1), both Sec45(A) and Sec45(B) (or Cys45 in the case of the mutant) remained in the secondary structure analogous to the crystal geometry. (The same output was found for their selenenic acid and selenylsulfide forms.) However, in a few cases (Table 1), a flip of the side chain of Sec45 occurred with a concomitant shift of the last turn at the N-terminal end of an α-helix (Figure 4a). This conformational change is described in Figure 4b by the disruption of a hydrogen bond between the backbone carbonyl oxygen of Thr47 of the last turn and the amide hydrogen of Asp42 of the neighboring turn of the α-helix. The flip was only observed in one monomer unit in the simulations either with the empty

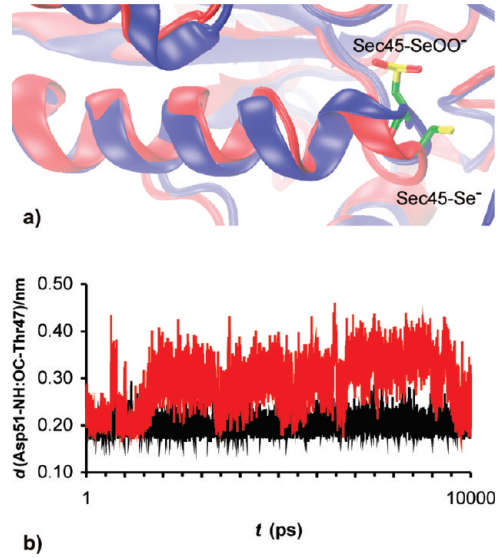


***Figure 4.*** (a) A superposition of a trajectory snapshot (from MD10_SeSG, red) with the crystal structure of GPx1 (PDB ID: 1GP1, blue). A flip of Sec45(B) (green) was only observed in a few trajectories. (b) A flip of Sec45(B) described by changes in interatomic distances *d*[Asp51(B)—NH···O=C—Thr47(B)] (red) during 10 ns MD simulation (MD10_SeSG). The Sec45(A) maintains a starting conformation *d*[Asp51(A)—NH···O=C—Thr47(A)] (black).

active site or with one bound GSH and with neutral or ionized redox states of Sec45 (Table 1). It was not observed in the simulations with two reduced GSHs bound at the active site. It is not clear whether this indicates a biophysical process involved in the redox mechanism of GPx1 or is only a transient conformation of the enzyme.

The conformational analysis of the positions of the side chain of Arg177 indicates a possible catalytic role of this residue in the redox cycle of GPx1 (Figure 5). During simulations, the side chain of Arg177 exhibited high flexibility (Figure 5e, f, and g), and its guanidinium moiety frequently stayed in proximity of Sec45 (3−5 Å). It is known that the positive electrostatic potential of arginine or other residues, such as lysine, can stabilize the ionic form of ionizable residues and cause a decreasing p$K_a$ value below 7 for residues, such as cysteine[38] (See also Figure 1d). Therefore, one catalytic role of Arg177 could be, besides the proper binding of GSH into the GPx1, the stabilization of the ionized selenolate of Sec45 and the thiolate state of GSH. Indeed, the side chain of Arg177 was often observed in the vicinity of the thiol group of GSH in our MD simulations (Figure 5). The importance of Arg residues in the reduction of hydrogen peroxide by a cysteine residue was recently demonstrated by QM calculations on the redox cycle of OxyR transcription factor.[38]

The His79(A) and His79(B) residues were found, both in the crystallographic measurements[3] and in our docking calculations, to interact with GSH. Their role is not clearly understood because they are not located in a reactive radius of Sec45(A) and Sec45(B) residues. They are part of the contact region of the monomer units, and the side chain of His79(A) is oriented toward Sec45(B), while His79(B) is toward Sec45(A). In 14 cases of 26 active sites analyzed,

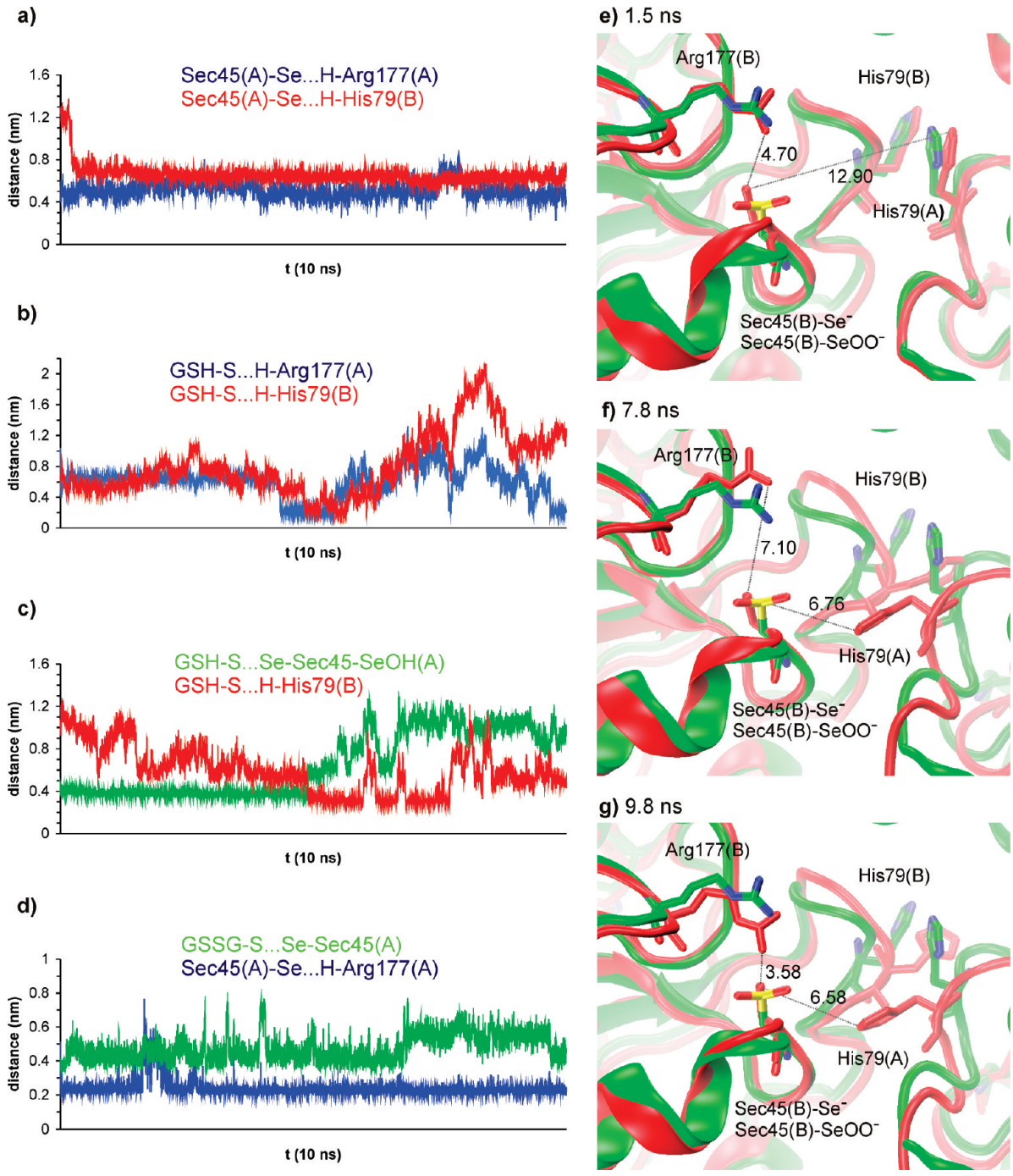


***Figure 5.*** Interatomic distances between selected amino acid residues of GPx1 and GSH from the MD trajectories. (a) MD1_Se; (b) MD8_SeO_GSH_GS_HIP; (c) MD5_SeOH_GSH; and (d) MD12_GSSG. Snapshots: (e) 1.5, (f) 7.8, and (g) 9.8 ns from MD1_Se (red) are superimposed with the crystal structure of GPx1 (PDB ID: 1GP1, green). High mobilities of the side chains of Arg177(B) and His79(A) are evident.

side chains of His79(A) [or His79(B)] remained in conformations similar to those found in the crystal structures of GPx1 (Table 1). In the remaining active site, we observed the movement of either the side chains of these histidines (12 cases, Figure 5f and g) or the histidines within the conformational change of the Asn75−Gln81 loop (13 cases). This conformation change was observed in the simulations either with the empty active site or with bound GSH. It was not observed in the simulations with two reduced GSHs bound at the active site (monomer A in MD2_Se_GSH_GSH, MD7_SeO_GSH_GSH, MD8_SeO_GSH_GS_HIP, and MD9_SeOH_GSH_GS_HIP, Table 1). A detailed structural analysis has shown that His79(A) [or His79(B)] moves to the vicinity of Sec45 as a consequence of the conformational change of the Asn75−Gln81 backbone. However, it should be noted that our simulations were performed for the dimer structure of GPx1, which misses in vivo tetrameric contact region. In the tetramer structure, the Asn75−Gln81 sequence could be more stabilized in a position analogous to the crystal structure. Therefore, we also performed MD simulations on the large tetramer structure of GPx1 (a 10 ns simulation with Sec45 in the selenolate state without bound GSHs). The

***Table 2.*** Comparison of Calculated and Experimental p$K_a$ Values of Selenols[a]

| compound | exptl.[b] | B3LYP[c] | MP2[c] | B3LYP[d] | B3LYP[e] | MP2[e] | B3LYP[f] |
|---|---|---|---|---|---|---|---|
| $H_2Se$ | 3.73 | 13.67 | 12.38 | 5.25 | 7.54 | 6.95 | 4.32 |
| $(CH_3)_2N-(CH_2)-SeH$ | 4.74 | 19.31 | 17.25 | 9.51 | 11.36 | 10.24 | 9.21 |
| $H_2N-CH_2-C(CH_3)_2-SeH$ | 5.21 | 19.76 | 17.80 | 10.84 | 12.43 | 10.40 | 9.52 |
| $H_2N-(CH_2)_2-SeH$ | 5.01 | 18.67 | 17.08 | 10.27 | 12.36 | 10.90 | 9.53 |
| $H_2N-(CH_2)_2-CH(CH_3)-SeH$ | 5.19 | 19.69 | 17.89 | 9.74 | 12.54 | 10.84 | 10.00 |
| selenocysteine | 5.24 | 18.26 | 16.38 | 8.41 | 10.42 | 9.27 | 8.07 |
| $r^2$ | | 0.83 | 0.84 | 0.74 | 0.75 | 0.71 | 0.79 |
| $k$ | | 0.23 | 0.26 | 0.25 | 0.26 | 0.33 | 0.24 |
| $d$ | | 0.66 | 0.63 | 2.61 | 1.95 | 1.65 | 2.80 |
| SE | | 0.27 | 0.26 | 0.33 | 0.32 | 0.35 | 0.30 |
| MAD | | 13.37 | 11.67 | 4.15 | 6.26 | 4.91 | 3.59 |

[a] SE is the standard error of the predicted p$K_a$; $r^2$ is the correlation coefficient; $k$ is the slope; $d$ is the intercept of correlation equation; and MAD is the mean value of ABS[p$K_a$(exp) − p$K_a$(calc)]. [b] Experimental p$K_a$ values are from refs 2, 82, and 83. [c] IEF-PCM; 6-31G(d,p). [d] IEF-PCM; aug-cc-pVDZ. [e] IEF-PCM; 6-31+G(d,p). [f] CPCM-COSMO-RS; 6-31+G(d,p).

***Table 3.*** Comparison of Calculated and Experimental p$K_a$ Values of Selenenic Acids[a]

| $2R^1$, $4R^2$−PheSeOH | exptl.[b] | B3LYP[c] | MP2[c] | B3LYP[d] | MP2[d] | B3LYP[e] | MP2[e] | B3LYP[f] |
|---|---|---|---|---|---|---|---|---|
| $R^1$=$R^2$=H | 11.50 | 31.79 | 33.18 | 20.41 | 19.07 | 20.04 | 19.17 | 16.09 |
| $R^1$=$NO_2$, $R^2$=H | 10.45 | 27.82 | 31.13 | 17.37 | 17.55 | 17.07 | 18.43 | 13.07 |
| $R^1$=$NO_2$, $R^2$=Cl | 10.17 | 26.32 | 30.00 | 16.36 | 16.83 | 16.07 | 17.23 | 12.22 |
| $R^1$=$NO_2$, $R^2$=$CH_3$ | 10.73 | 28.15 | 30.88 | 17.59 | 17.84 | 17.34 | 17.88 | 13.44 |
| $R^1$=$NO_2$, $R^2$=$CH_3O$ | 10.83 | 28.13 | 31.40 | 17.57 | —[g] | 17.22 | 19.36 | 13.41 |
| $r^2$ | | 0.94 | 0.92 | 0.93 | 0.99 | 0.93 | 0.57 | 0.95 |
| $k$ | | 0.24 | 0.41 | 0.32 | 0.61 | 0.33 | 0.42 | 0.33 |
| $d$ | | 3.91 | −2.12 | 5.05 | −0.14 | 5.04 | 2.94 | 6.18 |
| SE | | 0.14 | 0.16 | 0.15 | 0.08 | 0.15 | 0.38 | 0.13 |
| MAD | | 17.71 | 20.58 | 7.12 | 7.11 | 6.81 | 7.68 | 2.19 |

[a] SE is the standard error of the predicted p$K_a$; $r^2$ is the correlation coefficient; $k$ is the slope; $d$ is the intercept of correlation equation; and MAD is the mean value of ABS[p$K_a$(exp) − p$K_a$(calc)]. [b] Experimental p$K_a$ values from ref 85. [c] IEF-PCM; 6-31G(d,p). [d] IEF-PCM; aug-cc-pVDZ. [e] IEF-PCM; 6-31+G(d,p). [f] CPCM-COSMO-RS; 6-31+G(d,p). [g] Not converged.

Asn75−Gln81 loop in three subunits remained during the simulation in the position similar to the geometry of the crystal structure. In one subunit, a movement of the loop toward the active site, albeit in much less extent as it had been found in the simulations on the dimer of GPx1, was observed. This indicates: (i) the importance of the interactions between the two dimer units on the stability of GPx1; (ii) the observed conformational change of the Asn75−Gln81 loop is less frequent in the tetramer structure of GPx1 compared with our MD simulations on the dimer model of the enzyme; and (iii) the presence of two GSHs bound at the active site can probably stabilize the Asn75−Gln81 loop and His79 in a conformation similar to the crystal structure.

**3.3. p$K_a$ Calculations.** Before calculating p$K_a$ values for Sec45, calculations for a training set of organoselenium compounds, with available experimental p$K_a$ values,[2,82−85] were performed to test the accuracy of the methodology used.

Absolute values of calculated p$K_a$ substantially deviate from experimental data, trends for both selenols (Table 2) and selenenic acids (Table 3) are described with sufficient accuracy. Using larger basis sets augmented by diffuse functions significantly improved mean absolute deviations (MADs) by about 5−14 p$K_a$ units, however, standard errors of the calculated p$K_a$ values (SE = 0.26−0.27 p$K_a$ units for RSeH and 0.14−0.16 for RSeOH) and $r^2$ (0.83−0.84 for RSeH and 0.92−0.94 for RSeOH) slightly impaired by less than 0.1 units for RSeH and 0.3 for RSeOH (Tables 2 and 3). The results do not change significantly when the DFT method is substituted by an ab initio method (MP2). Although using the CPCM-COSMO-RS solvation model instead of IEFPCM significantly lowers the MADs, slopes and correlation coefficients are hardly affected. Similarly, inclusion of diffuse functions in the basis set is essential to obtain reasonable MADs, however, correlation coefficients and slopes ($k$ = 0.23−0.33 for both RSeH and RSeOH) are insensitive to either basis set or solvation model. As discussed by Kelly and co-workers,[63] implicit solvent models frequently give quite good correlations between calculated aqueous acid dissociation energies and experimental p$K_a$ values. The slopes of the regression lines are generally too low (around 0.5−0.6), and the authors conclude that inclusion of explicit solvent molecules is necessary. For instance, Adam[87] has successively added water molecules until a slope of 0.88/$RT$ln(10) for carboxylic acids could be attained. Kelly and co-workers[63] added a single explicit water molecule to anions with three or less atoms as well as to those with one or more oxygen atoms bearing a more negative partial charge than bare water. Table S2 in the Supporting Information presents the results obtained by adding one single $H_2O$ to the selenolate anions. There is a slight improvement in the correlation coefficients, however, the slopes are virtually unchanged and the MADs increase. If we add a single $H_2O$ only to those anions with a more negative charge on Se than on the water oxygen (data not shown), then even less agreement with experimental results is observed. A possible explanation for the low slopes might be the small spread of experimental p$K_a$ values within both series of compounds. Combining the two sets into one single correlation equation results in somewhat larger slopes, e.g. $k$ = 0.53 (IEFPCM-B3LYP/6-31G(d,p) (Table 4), comparable to those quoted

***Table 4.*** Statistical Results Obtained for the Merged Training Set[a]

| | IEF-PCM/ 6-31G(d,p) | IEF-PCM/ 6-31+G(d,p) | CPCM-COSMO-RS/ 6-31+G(d,p) |
|---|---|---|---|
| $r^2$ | 0.95 | 0.90 | 0.83 |
| $k$ | 0.53 | 0.79 | 0.88 |
| $d$ | −4.62 | −3.57 | −1.93 |
| SE | 0.72 | 1.02 | 1.36 |
| MAD | 15.34 | 6.51 | 3.28 |

[a] SE is the standard error of the predicted p$K_a$; $r^2$ is the correlation coefficient; $k$ is the slope; $d$ is the intercept of correlation equation; MAD is the mean value of ABS[p$K_a$(exp) − p$K_a$(calc)].

***Table 5.*** B3LYP Calculated Values of p$K_a$ of Sec45 in Aqueous Solution Using the Correlations Coefficients from Table 4

| | IEF-PCM/ 6-31G(d,p) | IEF-PCM/ 6-31+G(d,p) | CPCM-COSMO-RS/ 6-31+G(d,p) |
|---|---|---|---|
| Sec45−SeH | 3.72 ± 0.72 | 3.07 ± 1.02 | 4.30 ± 1.36 |
| Sec45−SeOH | 11.43 ± 0.72 | 12.10 ± 1.02 | 11.71 ± 1.36 |

by Klamt et al.,[81] Chipman,[88] and Klicić et al.[89] Even larger slopes are obtained when including diffuse functions in the basis set [B3LYP/6-31+G(d,p)], 0.79 (IEFPCM) and 0.88 (CPCM-COSMO-RS). Note that these slopes are directly comparable to those quoted by Kelly et al. (0.76 without explicit solvent and 0.87 when one water molecule added to some of the anions).[63] However, it must be stressed that the main goal of this paper was not to calculate absolute p$K_a$ values but rather to try to predict ionization states of Sec and its selenenic acid form in GPx1. Consequently, we used for the calculations of p$K_a$ of Sec45 and its selenenic acid form the equation: p$K_a$(exp) = $k$ × p$K_a$ (calc) + $d$, with correlation coefficients developed for the merged training set of the organoselenium compounds (Table 4).

The p$K_a$ values of the Sec45 residue were estimated at three levels, as they are compiled in Table 5. The estimated p$K_a$ values of Sec45 in aqueous solution are significantly lower (ca. 3−4) compared with the calculated value for the selenenic acid form (ca. 11−12) or with an experimentally measured value of cysteine (8.3).[2,25] These values are in the range of experimentally measured p$K_a$ values of selenocysteine in aqueous solution (5.3)[24] and the enzyme selenosubtilisin (p$K_a$ < 4).[26] We should note that p$K_a$ values calculated for Sec45 of GPx1 represent values for one enzyme conformation (see the Computational Details section). Due to the high mobility of the side chain of Arg177 as well as water molecules in a solvation shell of Sec45 observed in the MD simulations, the average p$K_a$ values of Sec45 and its selenenic acid form could slightly deviate from the calculated values. However, these results allowed us to propose that at a physiological pH of GPx1[3] (with the pH optimum of 8.8 and 8.5 measured for bovine and human GPx[90,91]) ionized and neutral forms of Sec45 are in dynamic equilibrium, in which selenolate can be preferred for the redox reaction with hydroperoxides because of its higher reactivity as a nucleophile. In contrast, the selenenic acid form of Sec45 would prefer the neutral protonated state for the second redox reaction with GSH. While in the first reaction with hydroperoxides the selenium atom acts a nucleophilic center, in the second reaction with GSH, selenenic acid switches to electrophilic one. Consequently, the ionized form of the selenenic acid, i.e., its low p$K_a$ value, would be undesirable to reach the electron-deficient selenium center necessary for attack of the GSH nucleophile.

Our results support the generally proposed redox mechanism of GPx1 (Figure 1a) that selenocysteine reacts with hydroperoxides as a selenolate and that a donor proton must be supplied. According to the MD simulations, the dyad Arg177−His79 could play the role of proton supplier in the redox cycle of GPx1 (Figure 1c).

## Conclusion

Using three different tools of computational chemistry we have revealed some missing structural information concerning the redox cycle of GPx1. Based on p$K_a$ calculations, the resting form of the catalytic Sec45 is allowed to be in selenolate (E−Se$^-$) at in vivo pH. This form is more reactive toward hydroperoxides,[17,18,92,93] thus increasing catalytic effectiveness of GPx1. Its transient selenenic acid form prefers the neutral state (E−SeOH) because Sec switches from nucleophile to electrophile in the second redox step of the GPx1 cycle. According to docking and MD simulations, Arg177, His79, Phe145, and primarily Trp158 seem to play a key role in the binding and proper orientation of the thiol group of GSH toward the selenocysteine reaction center. The MD simulations indicated that Arg177 and His79 could be involved in the catalytic cycle of GPx1, however, their exact chemical roles were not able to be deduced from the classical molecular mechanics (MM) simulations. We propose that Arg177 can maintain an increased positive electrostatic potential around the reaction center necessary for stabilizing the ionized states of Sec45 and GSH (Figure 1d), and together with His79 could be involved in proton transfer in the reaction steps of the GPx1 cycle (Figure 1c). To validate the redox mechanism of GPx1 with the Agr177−His79 catalytic dyad, further calculations at high quantum mechanics and QM/MM levels are needed.

**Acknowledgment.** Financial support for this research was granted by the Action Austria-Slovakia and the Centers of Excellence program of the Slovak Academy of Sciences (COMCHEM, Contract no. II/1/2007). J.K. acknowledges financial support from the Slovak Research and Development Agency, APVV (0117-06), and a VEGA grant 2/0176/09. We also thank to Dr. Otyepka from Palacký University in Olomouc for the support with programs for building and analyzing the structures from the ONIOM calculations.

**Supporting Information Available:** Gaussian input files of optimized structures, docked structures of the complexes GPx1:GSH:GSH, GPx1:GSH:GS, and GPx1:GSSG, an output structure from the PropKa calculations, force field parameters for the Sec residue, GSH and all their redox states. This information is available free of charge via the Internet at http://pubs.acs.org/.

### References

(1) Flohé, L.; Gunzler, W. A.; Schock, H. H. *FEBS Lett.* **1973**, *32*, 132.

(2) Johansson, L.; Gafvelin, G.; Arner, E. S. J. *Biochim. Biophys. Acta* **2005**, *1726*, 1.

(3) Epp, O.; Ladenstein, R.; Wendel, A. *Eur. J. Biochem.* **1983**, *133*, 51.

(4) Gettins, P.; Crews, B. C. *J. Biol. Chem.* **1991**, *266*, 4804.

(5) Maiorino, M.; Aumann, K. D.; Brigelius-Flohe, R.; Doria, D.; van den Heuvel, J.; McCarthy, J.; Roveri, A.; Ursini, F.; Flohe, L. *Z. Ernährungswiss.* **1998**, *37*, 118.

(6) Rocher, C.; Lalanne, J. L.; Chaudiere, J. *Eur. J. Biochem.* **1992**, *205*, 955.

(7) Ren, B.; Huang, W. H.; Akesson, B.; Ladenstein, R. *J. Mol. Biol.* **1997**, *268*, 869.

(8) Flohé, L.; Loschen, G.; Gunzler, W. A.; Eichele, E. *Hoppe-Seyler's Z. Physiol. Chem.* **1972**, *353*, 987.

(9) Mugesh, G.; du Mont, W. W.; Sies, H. *Chem. Rev.* **2001**, *101*, 2125.

(10) Prabhakar, R.; Vreven, T.; Morokuma, K.; Musaev, D. G. *Biochemistry* **2005**, *44*, 11864.

(11) Prabhakar, R.; Vreven, T.; Frisch, M. J.; Morokuma, K.; Musaev, D. G. *J. Phys. Chem. B* **2006**, *110*, 13608.

(12) Prabhakar, R.; Musaev, D. G.; Khavrutskii, I. V.; Morokuma, K. *J. Phys. Chem. B* **2004**, *108*, 12643.

(13) Bayse, C. A. *J. Phys. Chem. A* **2007**, *111*, 9070.

(14) Bayse, C. A.; Antony, S. *Main Group Chem.* **2007**, *6*, 185.

(15) Bayse, C. A.; Antony, S. *J. Phys. Chem. A* **2009**, *113*, 5780.

(16) Bayse, C. A. *J. Inorg. Biochem.* **2010**, *104*, 1.

(17) Cardey, B.; Enescu, M. *J. Phys. Chem. A* **2007**, *111*, 673.

(18) Cardey, B.; Enescu, M. *ChemPhysChem* **2005**, *6*, 1175.

(19) Bachrach, S. M.; Walker, C. J.; Lee, F.; Royce, S. *J. Org. Chem.* **2007**, *72*, 5174.

(20) Bachrach, S. M.; Demoin, D. W.; Luk, M.; Miller, J. V. *J. Phys. Chem. A* **2004**, *108*, 4040.

(21) Hayes, J. M.; Bachrach, S. M. *J. Phys. Chem. A* **2003**, *107*, 7952.

(22) Bachrach, S. M.; Woody, J. T.; Mulhearn, D. C. *J. Org. Chem.* **2002**, *67*, 8983.

(23) Bach, R. D.; Dmitrenko, O.; Thorpe, C. *J. Org. Chem.* **2008**, *73*, 12.

(24) Tan, K. S.; Arnold, A. P.; Rabenstein, D. L. *Can. J. Chem.* **1988**, *66*, 54.

(25) Huber, R. E.; Criddle, R. S. *Arch. Biochem. Biophys.* **1967**, *122*, 164.

(26) House, K. L.; Dunlap, R. B.; Odom, J. D.; Wu, Z. P.; Hilvert, D. *J. Am. Chem. Soc.* **1992**, *114*, 8573.

(27) Syed, R.; Wu, Z. P.; Hogle, J. M.; Hilvert, D. *Biochemistry* **1993**, *32*, 6157.

(28) Yang, Z.; Zhou, C. Z. *Acta Crystallogr., Sect. F: Struct. Biol. Cryst. Commun.* **2006**, *62*, 593.

(29) Scheerer, P.; Borchert, A.; Krauss, N.; Wessner, H.; Gerth, C.; Hohne, W.; Kuhn, H. *Biochemistry* **2007**, *46*, 9041.

(30) Claiborne, A.; Yeh, J. I.; Mallett, T. C.; Luba, J.; Crane, E. J.; Charrier, V.; Parsonage, D. *Biochemistry* **1999**, *38*, 15407.

(31) Poole, L. B.; Nelson, K. J. *Curr. Opin. Chem. Biol.* **2008**, *12*, 18.

(32) Salmeen, A.; Andersen, J. N.; Myers, M. P.; Meng, T. C.; Hinks, J. A.; Tonks, N. K.; Barford, D. *Nature* **2003**, *423*, 769.

(33) van Montfort, R. L. M.; Congreve, M.; Tisi, D.; Carr, R.; Jhoti, H. *Nature* **2003**, *423*, 773.

(34) Brandt, W.; Wessjohann, L. A. *ChemBioChem* **2005**, *6*, 386.

(35) Sarma, B. K.; Mugesh, G. *Inorg. Chem.* **2006**, *45*, 5307.

(36) Sandalova, T.; Zhong, L. W.; Lindqvist, Y.; Holmgren, A.; Schneider, G. *Proc. Nat. Acad. Sci. U.S.A.* **2001**, *98*, 9533.

(37) Roy, G.; Sarma, B. K.; Phadnis, P. P.; Mugesh, G. *J. Chem. Sci.* **2005**, *117*, 287.

(38) Kóňa, J.; Brinck, T. *Org. Biomol. Chem.* **2006**, *4*, 3468.

(39) Zheng, M.; Aslund, F.; Storz, G. *Science* **1998**, *279*, 1718.

(40) Kavanagh, K. L.; Johansson, C.; Smee, C.; Gileadi, O.; Von Delft, F.; Weigelt, C. J.; Sundstrom, M.; Edwards, A.; Oppermann, U. Crystal structure of the selenocysteine to glycine mutant of human glutathione peroxidase 1; The Research Collaboratory for Structural Bioinformatics (RCSB): RCSB-Rutgers, RCSB-San Diego Supercomputer Center, and RCSB-University of Wisconsin-Madison; http://www.rcsb.org/. Accessed May 22, 2009.

(41) *Glide*, version 4.5; Schrödinger, LLC: New York, NY, 2007.

(42) *MacroModel*, version 9.5; Schrödinger, LLC: New York, NY, 2007.

(43) Kaminski, G. A.; Friesner, R. A.; Tirado-Rives, J.; Jorgensen, W. L. *J. Phys. Chem. B* **2001**, *105*, 6474.

(44) Jorgensen, W. L.; Maxwell, D. S.; Tirado-Rives, J. *J. Am. Chem. Soc.* **1996**, *118*, 11225.

(45) Friesner, R. A.; Murphy, R. B.; Repasky, M. P.; Frye, L. L.; Greenwood, J. R.; Halgren, T. A.; Sanschagrin, P. C.; Mainz, D. T. *J. Med. Chem.* **2006**, *49*, 6177.

(46) Friesner, R. A.; Banks, J. L.; Murphy, R. B.; Halgren, T. A.; Klicic, J. J.; Mainz, D. T.; Repasky, M. P.; Knoll, E. H.; Shelley, M.; Perry, J. K.; Shaw, D. E.; Francis, P.; Shenkin, P. S. *J. Med. Chem.* **2004**, *47*, 1739.

(47) *Maestro*, version 8.0; Schrödinger, LLC: New York, NY, 2007.

(48) Jorgensen, W. L.; Chandrasekhar, J.; Madura, J. D.; Impey, R. W.; Klein, M. L. *J. Chem. Phys.* **1983**, *79*, 926.

(49) van der Spoel, D.; Lindahl, E.; Hess, B.; van Buuren, A. R.; Apol, E.; Meulenhoff, P. J.; Tieleman, D. P.; Sijbers, A. L. T. M.; Feenstra, K. A.; van Drunen, R.; Berendsen, H. J. C. *Gromacs 3.3.1*; Department of Biophysical Chemistry, University of Groningen: Groningen, The Netherlands, 2004.

(50) Roothaan, C. C. J. *Rev. Mod. Phys.* **1951**, *23*, 69.

(51) Frisch, M. J.; Trucks, G. W.; Schlegel, H. B.; Scuseria, G. E.; Robb, M. A.; Cheeseman, J. R.; Montgomery Jr., J. A.; Vreven, T.; Kudin, K. N.; Burant, J. C.; Millam, J. M.; Iyengar, S. S.; Tomasi, J.; Barone, V.; Mennucci, B.; Cossi, M.; Scalmani, G.; Rega, N.; Petersson, G. A.; Nakatsuji, H.; Hada, M.; Ehara, M.; Toyota, K.; Fukuda, R.; Hasegawa, J.; Ishida, M.; Nakajima, T.; Honda, Y.; Kitao, O.; Nakai, H.; Klene, M.; Li, X.; Knox, J. E.; Hratchian, H. P.; Cross, J. B.; Bakken, V.; Adamo, C.; Jaramillo, J.; Gomperts, R.; Stratmann, R. E.; Yazyev, O.; Austin, A. J.; Cammi, R.; Pomelli, C.; Ochterski, J. W.; Ayala, P. Y.; Morokuma, K.; Voth, G. A.; Salvador, P.; Dannenberg, J. J.; Zakrzewski, V. G.; Dapprich, S.; Daniels, A. D.; Strain, M. C.; Farkas, O.; Malick, D. K.;

Rabuck, A. D.; Raghavachari, K.; Foresman, J. B.; Ortiz, J. V.; Cui, Q.; Baboul, A. G.; Clifford, S.; Cioslowski, J.; Stefanov, B. B.; Liu, G.; Liashenko, A.; Piskorz, P.; Komaromi, I.; Martin, R. L.; Fox, D. J.; Keith, T.; Al-Laham, M. A.; Peng, C. Y.; Nanayakkara, A.; Challacombe, M.; Gill, P. M. W.; Johnson, B.; Chen, W.; Wong, M. W.; Gonzalez, C.; Pople, J. A. *Gaussian 03*, revision D.02 and E.01; Gaussian, Inc.: Wallingford, CT, 2005.

(52) Besler, B. H.; Merz, K. M., Jr.; Kollman, P. A. *J. Comput. Chem.* **1990**, *11*, 431.

(53) Singh, U. C.; Kollman, P. A. *J. Comput. Chem.* **1984**, *5*, 129.

(54) Bas, D. C.; Rogers, D. M.; Jensen, J. H. *Proteins* **2008**, *73*, 765.

(55) Li, H.; Robertson, A. D.; Jensen, J. H. *Proteins* **2005**, *61*, 704.

(56) Berendsen, H. J. C.; Postma, J. P. M.; van Gunsteren, W. F.; Dinola, A.; Haak, J. R. *J. Chem. Phys.* **1984**, *81*, 3684.

(57) Darden, T.; York, D.; Pedersen, L. *J. Chem. Phys.* **1993**, *98*, 10089.

(58) Hess, B.; Bekker, H.; Berendsen, H. J. C.; Fraaije, J. *J. Comput. Chem.* **1997**, *18*, 1463.

(59) Schafmeister, C. E. A. F.; Ross, W. S.; Romanovski, V. *LEAP*; University of California: San Francisco, 1995.

(60) Case, D. A.; Darden, T. A.; Cheatham , T. E., III; Simmerling, C. L.; Wang, J.; Duke, R. E.; Luo, R.; Merz, K. M.; Wang, B.; Pearlman, D. A.; Crowley, M.; Brozell, S.; Tsui, V.; Gohlke, H.; Mongan, J.; Hornak, V.; Cui, G.; Beroza, P.; Schafmeister, C.; Caldwell, J. W.; Ross, W. S.; Kollman, P. A. *Amber 8*; University of California: San Francisco, 2004.

(61) Sadlej-Sosnowska, N. *Theor. Chem. Acc.* **2007**, *118*, 281.

(62) Wang, X. X.; Fu, H.; Du, D. M.; Zhou, Z. Y.; Zhang, A. G.; Su, C. F.; Ma, K. S. *Chem. Phys. Lett.* **2008**, *460*, 339.

(63) Kelly, C. P.; Cramer, C. J.; Truhlar, D. G. *J. Phys. Chem. A* **2006**, *110*, 2493.

(64) Hudaky, P.; Perczel, A. *J. Phys. Chem. A* **2004**, *108*, 6195.

(65) Palascak, M. W.; Shields, G. C. *J. Phys. Chem. A* **2004**, *108*, 3692.

(66) Tissandier, M. D.; Cowen, K. A.; Feng, W. Y.; Gundlach, E.; Cohen, M. H.; Earhart, A. D.; Coe, J. V.; Tuttle, T. R. *J. Phys. Chem. A* **1998**, *102*, 7787.

(67) Vreven, T.; Byun, K. S.; Komáromi, I.; Dapprich, S.; Montgomery, J. A., Jr.; Morokuma, K.; Frisch, M. J. *J. Chem. Theory Comput.* **2006**, *2*, 815.

(68) Dapprich, S.; Komáromi, I.; Byun, K. S.; Morokuma, K.; Frisch, M. J. *J. Mol. Struct. THEOCHEM* **1999**, *462*, 1.

(69) Tomasi, J.; Mennucci, B.; Cances, E. *J. Mol. Struct. THEOCHEM* **1999**, *464*, 211.

(70) Namazian, M.; Zakery, M.; Noorbala, M. R.; Coote, M. L. *Chem. Phys. Lett.* **2008**, *451*, 163.

(71) Lim, C.; Bashford, D.; Karplus, M. *J. Phys. Chem.* **1991**, *95*, 5610.

(72) Bryantsev, V. S.; Diallo, M. S.; Goddard, W. A. *J. Phys. Chem. A* **2007**, *111*, 4422.

(73) Schmidt am Busch, M.; Knapp, E. W. *ChemPhysChem* **2004**, *5*, 1513.

(74) Becke, A. D. *J. Chem. Phys.* **1993**, *98*, 5648.

(75) Lee, C. T.; Yang, W. T.; Parr, R. G. *Phys. Rev. B: Condens. Matter Mater. Phys.* **1988**, *37*, 785.

(76) Hariharan, P. C.; Pople, J. A. *Theor. Chim. Acta* **1973**, *28*, 213.

(77) Clark, T.; Chandrasekhar, J.; Spitznagel, G. W.; von Ragué Schleyer, P. *J. Comput. Chem.* **1983**, *4*, 294.

(78) Krishnan, R.; Binkley, J. S.; Seeger, R.; Pople, J. A. *J. Chem. Phys.* **1980**, *72*, 650.

(79) Dunning, T. H. *J. Chem. Phys.* **1989**, *90*, 1007.

(80) Møller, C.; Plesset, M. S. *Phys. Rev.* **1934**, *46*, 618.

(81) Klamt, A.; Jonas, V.; Burger, T.; Lohrenz, J. C. W. *J. Phys. Chem. A* **1998**, *102*, 5074.

(82) Sokolov, M. N.; Abramov, P. A.; Peresypkina, E. V.; Virovets, A. V.; Fedin, V. P. *Polyhedron* **2008**, *27*, 3259.

(83) Yokoyama, A.; Sakurai, H.; Tanaka, H. *Chem. Pharm. Bull.* **1970**, *19*, 1089.

(84) Kurz, J. L.; Harris, J. C. *J. Org. Chem.* **1970**, *35*, 3086.

(85) Kang, S. I.; Kice, J. L. *J. Org. Chem.* **1986**, *51*, 287.

(86) Sarma, B. K.; Mugesh, G. *Org. Biomol. Chem.* **2008**, *6*, 965.

(87) Adam, K. R. *J. Phys. Chem. A* **2002**, *106*, 11963.

(88) Chipman, D. M. *J. Phys. Chem. A* **2002**, *106*, 7413.

(89) Klicić, J. J.; Friesner, R. A.; Liu, S.-Y.; Guida, W. C. *J. Phys. Chem. A* **2002**, *106*, 1327.

(90) Wendel, A. *Methods Enzymol.* **1981**, *77*, 325.

(91) Rey, C.; Véricel, E.; Némoz, G.; Chen, W.; Chapuy, P.; Lagarde, M. *Biochim. Biophys. Acta* **1994**, *1226*, 219.

(92) Benková, Z.; Kóňa, J.; Gann, G.; Fabian, W. M. F. *Int. J. Quantum Chem.* **2002**, *90*, 555.

(93) Pearson, J. K.; Boyd, R. J. *J. Phys. Chem. A* **2007**, *111*, 3152.

CT9003355